Proceedings of the 28th IEEE
EMBS Annual International Conference
New York City, USA, Aug 30-Sept 3, 2006

Maximum-Likelihood Estimation of Detector Response for PET Image Reconstruction

Jinyi Qi

Abstract— **An accurate system model is essential for reconstructing high-resolution images. While the system response of a positron emission tomography (PET) system can be measured directly, the process is often difficult to perform and time-consuming. Here we propose a maximum likelihood method for estimating the detector response from projections of a point source at a set of radial locations in the field of view. The detector response functions for all radial bins are estimated simultaneously. No interpolation is required. Compared to the method of direct measurement, the proposed approach requires less measurements and results in sparse system matrix because a factored system matrix is used, which reduces the reconstruction time. We conducted computer simulation to demonstrate the feasibility of the proposed method.**

I. INTRODUCTION

Iterative image reconstruction methods have gained increasing popularity in emission tomography because they are amendable to an arbitrary, complicated, and realistic system model that defines the mapping from sources to measurements. It is been shown in both positron emission tomography (PET) and single photon emission computed tomography (SPECT) that accurately modeling the system response leads to improved image quality. Clinical studies also show improved sensitivity and specificity in the diagnosis and evaluation of coronary artery disease [1], [2].

In PET resolution is affected by the combined effects of positron range, noncolinearity of the photon pair, variations in detector-pair sensitivity along the line of response (LOR), and the spatially variant response of the detector caused by intercrystal penetration and scatter. The resolution in filtered backprojection degrades significantly as the target is moved from the center of the scanner to radially off-center locations. By modeling these effects in an iterative reconstruction framework, one can achieve nearly uniform resolution across the field of view (FOV).

One approach to obtaining an accurate PET model is measuring it directly by scanning a small point source covering the FOV [3], [4]. This method can be time-consuming and storing the resulting system matrix can also be challenging. Alternatively, the system matrix can be factored into a product of a geometric projection matrix and a detector response matrix [5], [6]. The geometric projection matrix can be calculated based on the solid angle effect in coincidence detection. It is highly sparse and can be stored efficiently. The detector response matrix models the local blurring in sinogram space. It is sparse and rotationally symmetric. Thus the storage is not a problem. In SPECT detector response can be measured easily because there is no crosstalk between projections taken from different view angles [7]–[9]. However, measuring detector response in PET requires a collimated source because of the crosstalk between adjacent projection angles. As a result, Monte Carlo simulations are often used [5], [6], [10].

In order to use measurements of an uncollimated point source to calculate the detector response, Alessio *et al* [11] assumed that detector response was confined in radial direction only. The radial profiles of the measured point source projection are parameterized using discrete cosine transform. A linear fit amongst all the coefficients were used to calculate the response functions at other radial locations. Frese *et al* [12] measured detector response using a line source by assuming that the response function is constant for all lines of response.

In this paper we present a maximum likelihood (ML) method for estimating the detector response function from uncollimated point source measurements. We model the detector response of a 2D PET as a spatially variant 2D filter in sinogram space. An iterative ML algorithm is developed to estimate the detector response functions for all sinogram elements. No interpolation is required. Beekman *et al* [13] also used a ML method to estimate the detector response in SPECT from measurements of an extended source. Our focus is on PET, which has very different geometry and detector response model from SPECT.

II. THEORY

A. Log Likelihood Function

We estimate the detector response in PET from point source measurements using the maximum-likelihood principle. PET data are modeled as a collection of independent Poisson random variables with mean $\bar{\boldsymbol{y}}$ equal to

$$\bar{\boldsymbol{y}} = \boldsymbol{P}\boldsymbol{x} + \boldsymbol{r}, \tag{1}$$

where $\boldsymbol{P} \in \mathbb{R}^{M \times N}$ is the system matrix with the (i,j)th element equal to the probability of detecting an event from the jth voxel at the ith measurement and $\boldsymbol{r} \in \mathbb{R}^{M \times 1}$ accounts for the presence of scattered and random events in the data. In point source measurements $\boldsymbol{r}$ is considered as negligible. In [5], [6] the system matrix $\boldsymbol{P}$ is factored into

$$\boldsymbol{P} = \boldsymbol{P}_{\text{sens}} \boldsymbol{B} \boldsymbol{P}_{\text{attn}} \boldsymbol{P}_{\text{geom}}, \tag{2}$$

where $\boldsymbol{P}_{\text{geom}}$ is a geometric projection matrix with element (i,j) equal to the probability of a photon pair produced in

This work was supported by NIH R01 EB000194.

J. Qi is with the Department of Biomedical Engineering, University of California, Davis, CA 95616, USA (qi@ucdavis.edu).

voxel j reaching the surfaces of detector pair i in the absence of attenuation, $\boldsymbol{B}$ is the detector response matrix that models the crystal penetration, intercrystal scatter, and other blurring effects in photon detection. The diagonal matrices $\boldsymbol{P}_{\text{attn}}$ and $\boldsymbol{P}_{\text{sens}}$ account for the photon attenuation inside the object and the variation of the detector sensitivities, respectively. $\boldsymbol{P}_{\text{geom}}$ is calculated based on the solid angle effect [6]. $\boldsymbol{P}_{\text{attn}}$ and $\boldsymbol{P}_{\text{sens}}$ are measured with standard blank, transmission, and normalization scans.

Here we focus on estimating $\boldsymbol{B}$. The log likelihood function can be written as

$$\begin{aligned} L(\boldsymbol{B}) &= \log p(\boldsymbol{y}; \boldsymbol{g}, \boldsymbol{B}) \\ &= \sum_{m=1}^{M} \sum_{i=1}^{N} y_{i,m} \log(n_i \sum_{j=1}^{N} b_{ij} g_{j,m}) - n_i \sum_{j=1}^{N} b_{ij} g_{j,m}, \end{aligned} \tag{3}$$

where $y_{i,m}$ and $g_{i,m}$ are the measured projection and calculated geometric projection of the mth point source at LOR i, respectively, b_{ij} is the (i,j)th element of $\boldsymbol{B}$, and n_i is the detector sensitivity factor for LOR i. The geometric projection $g_{j,m}$ is defined as

$$g_{j,m} = a_j \sum_{k=1}^{N} P_{\text{geom}}(j,k) x_{k,m}, \tag{4}$$

where a_j is the attenuation factor for the jth LOR and $x_{k,m}$ is the image of the mth point source with k as the pixel index. In this work $g_{j,m}$ are known. The goal is to estimate b_{ij} from a given set of point source measurements $y_{i,m}$. We use a ML estimator, i.e.

$$\hat{\boldsymbol{B}} = \arg\max_{\boldsymbol{B}} L(\boldsymbol{B}), \tag{5}$$

subject to

$$b_{ij} \geq 0,\ i = 1, \ldots, N,\ j = 1, \ldots, N.$$

The first and second derivatives of the log likelihood function are

$$\frac{\partial L}{\partial b_{ij}} = \sum_{m=1}^{M} \frac{y_i g_{j,m}}{\sum_{j'=1}^{N} b_{ij'} g_{j',m}} - n_i g_{j,m} \tag{6}$$

$$\frac{\partial^2 L}{\partial b_{ij} \partial b_{kl}} = -\sum_{m=1}^{M} \delta(i-k) \frac{y_i g_{j,m} g_{l,m}}{(\sum_{j'=1}^{N} b_{ij'} g_{j',m})^2} \tag{7}$$

where $\delta(n)$ is the Kronecker delta function. It is easy to show that

$$\begin{aligned} \sum_{i,j,k,l} c_{ij} c_{kl} \frac{\partial^2 L}{\partial b_{ij} \partial b_{kl}} &= -\sum_{i,j,k,l,m} c_{ij} c_{kl} \frac{\delta(i-k) y_i g_{j,m} g_{l,m}}{(\sum_{j'=1}^{N} b_{ij'} g_{j',m})^2} \\ &= -\sum_{i,m} \frac{y_i (\sum_j c_{ij} g_{j,m})^2}{(\sum_{j'=1}^{N} b_{ij'} g_{j',m})^2} \\ &\leq 0 \end{aligned} \tag{8}$$

Therefore the log-likelihood function is concave.

B. Optimization

We use the optimization transfer principle to derive a monotonic optimization algorithm. Using the concavity of the $\log(\cdot)$ function, we have

$$\begin{aligned} \log(n_i \sum_{j=1}^{N} b_{ij} g_j) &= \log(n_i \sum_{j=1}^{N} \alpha_{ij} \frac{b_{ij} g_j}{\alpha_{ij}}) \\ &\geq \sum_{j=1}^{N} \alpha_{ij} \log(\frac{n_i b_{ij} g_j}{\alpha_{ij}}), \end{aligned} \tag{9}$$

for any

$$\sum_{j=1}^{N} \alpha_{ij} = 1,\ \alpha_{ij} \geq 0. \tag{10}$$

Choosing

$$\alpha_{ij} = \frac{b_{ij}^n g_j}{\sum_{j'=1}^{N} b_{ij'}^n g_{j'}}, \tag{11}$$

we obtain a separable surrogate function for the log likelihood function

$$\phi(\boldsymbol{B}; \boldsymbol{B}^n) = \sum_{m=1}^{M} \phi_m(\boldsymbol{B}; \boldsymbol{B}^n), \tag{12}$$

$$\begin{aligned} \phi_m(\boldsymbol{B}; \boldsymbol{B}^n) = &\sum_{i,j} \frac{b_{ij}^n y_{i,m} g_{j,m}}{\sum_{j'} b_{ij'}^n g_{j',m}} \log\left(\frac{n_i b_{ij} \sum_{j'} b_{ij'}^n g_{j',m}}{b_{ij}^n} \right) \\ &- \sum_{i=1}^{N} n_i \sum_{j=1}^{N} b_{ij} g_{j,m}. \end{aligned}$$

It is easy to verify that $\phi(\boldsymbol{B}; \boldsymbol{B}^n)$ satisfies the surrogate conditions

$$\phi(\boldsymbol{B}^n; \boldsymbol{B}^n) = L(\boldsymbol{B}^n) \tag{13}$$

$$\phi(\boldsymbol{B}; \boldsymbol{B}^n) \leq L(\boldsymbol{B}). \tag{14}$$

Maximizing (12) with respect to b_{ij} by setting the derivative

$$\frac{\partial \phi}{\partial b_{ij}} = \sum_{m=1}^{M} \frac{b_{ij}^n y_{i,m} g_{j,m}}{\sum_{j'=1}^{N} b_{ij'}^n g_{j',m}} \frac{1}{b_{ij}} - n_i g_{j,m} \tag{15}$$

to zero, we get a closed-form update equation

$$b_{ij}^{n+1} = \frac{b_{ij}^n}{n_i \sum_{m=1}^{M} g_{j,m}} \sum_{m=1}^{M} \frac{y_{i,m} g_{j,m}}{\sum_{j'=1}^{N} b_{ij'}^n g_{j',m}}. \tag{16}$$

Since the log-likelihood function is concave, the sequence generated by (16) monotonically converges to an ML solution. The nonnegativity constraint is also implicitly guaranteed. The algorithm in (16) is very similar to the emission ML expectation-maximization (EM) algorithm.

C. Rotational Symmetry

Most PET scanners have detectors forming a ring. Thus the detector blurring function $\boldsymbol{B}$ is rotational symmetric. Let us index sinogram element i by two coordinates (i_r, i_φ), where $i_r = 1, \ldots, N_r$ is the radial index and $i_\varphi = 1, \ldots, N_\varphi$ is the

angular index. Let us index b_{ij} using $b(i_r, i_\varphi, j_r, j_\varphi)$. The rotation symmetry can be written as

$$b(i_r, i_\varphi, j_r, j_\varphi) = b(i_r, 0, j_r, j_\varphi - i_\varphi). \quad (17)$$

Using (17) we can reduce the number of unknown in $\boldsymbol{B}$ by a factor of N_φ and improve the stability of the ML estimation. The new update equation with consideration of (17) is

$$b^{n+1}(i_r, 0, j_r, d\varphi) = \frac{b^n(i_r, 0, j_r, d\varphi)}{\sum_{i_\varphi=1}^{N_\varphi} n_{i_r,i_\varphi} \sum_{m=1}^{M} g_{j_r,i_\varphi+d\varphi,m}} \sum_{i_\varphi=1}^{N_\varphi} \sum_{m=1}^{M} \frac{y_{i_r,i_\varphi,m} g_{j_r,i_\varphi+d\varphi,m}}{\sum_{j'=1}^{N} b^n_{i_r,i_\varphi,j'} g_{j',m}}. \quad (18)$$

D. Variance

Without the nonnegativity constraint, the variance of the ML solution can be approximately estimated using the Cramer-Rao bound, which is the equal to the inverse of the Fisher information matrix. For the log-likelihood function in (3), the (u, v)th element of the Fisher information matrix is

$$\boldsymbol{F}_{uv} = -E\left[\frac{\partial^2 L(\boldsymbol{B})}{\partial b_{ij} \partial b_{kl}}\right]_{\boldsymbol{B}=\hat{\boldsymbol{B}}} = \sum_m \frac{g_{j,m} g_{l,m}}{\bar{y}_{i,m}} \delta(i-k), \quad (19)$$

where $u = I \times N + j$, $v = k \times N + l$, and $\bar{y}_{i,m} = \sum_j b_{ij} g_{j,m}$. Since F_{uv} is nonzero only when $i = k$, $\boldsymbol{F}$ is a block diagonal matrix, of which the inverse can be easily computed.

When considering rotational symmetry, the size of $\boldsymbol{F}$ is reduced by N_φ in each dimension. The (u', v')th element of the new Fisher information matrix is

$$\boldsymbol{F}_{u'v'} = \sum_{i_\varphi} \sum_m \frac{g_{j_r,i_\varphi+d\varphi_1,m} g_{l_r,i_\varphi+d\varphi_2,m}}{\bar{y}_{i_r,i_\varphi,m}} \delta(i_r - k_r), \quad (20)$$

where $u' = (i_r \times N_r + j_r)N_\varphi + d\varphi_1$ and $v' = (k_r \times N_r + l_r)N_\varphi + d\varphi_2$.

E. Implementation Considerations

Since the detector blurring is a local operation, most elements in $b(i_r, 0, j_r, d\varphi)$ are zero for $|i_r - j_r| \geq K_r$ or $|d\varphi| \geq K_\varphi$, where $K_r \ll N_r$ and $K_\varphi \ll N_\varphi$ are some positive integers. Thus the calculation in (18) can be limited to $|i_r - j_r| < K_r$ and $|d\varphi| < K_\varphi$, which reduces the computation cost without affecting the accuracy of the estimate.

III. Computer Simulation

We apply the propose method to a simulated 2D PET system. The simulated PET scanner has 240 detectors uniformly spaced on a ring of diameter 152 mm (Fig. 1). The dimension of each detector crystal is 2 mm (transaxial) × 3 mm (axial) × 20 mm (radial). The scintillation material is LSO.

The geometric projection matrix is calculated by assuming the detectors to be "black" (i.e. attenuation length being zero). The true point source projections are generated using a Monte Carlo simulation program [14]. Fig. 2 shows the comparison of the geometric projections and true projections of a point source at six radial locations. Because of the crystal penetration effect, the true projections are blurred at large radial offsets.

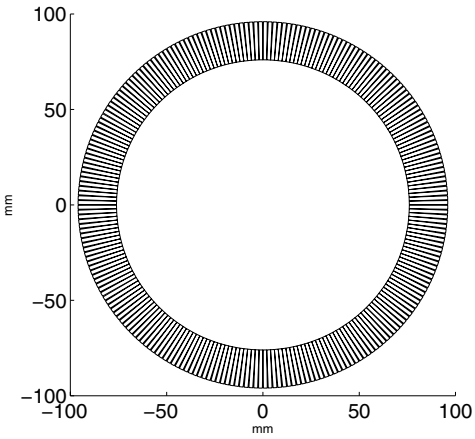

Fig. 1. The simulated 2D PET system with 240 individual detectors.

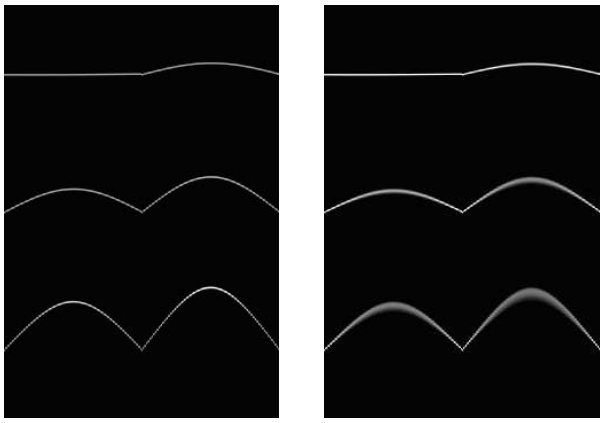

(a) (b)

Fig. 2. The geometric projections (a) and true projections (b) of a point source at six radial offsets: 0 mm (center), 10 mm, 20 mm, 30 mm, 40 mm, and 50 mm.

We used the propose method to estimate the detector response from the true point source projections. Fig. 3(a) shows estimated detector response function at eight selected radial bins. Note that the detector responses are shift variant two-dimensional blurring function. Fig. 3(b) shows the fitted point source projections using the estimate detector response function. The results are very similar to the true projections shown in Fig. 2(b). In Fig. 4 we compare the radial profiles of the true projections, geometric projections, and fitted projections of a point source at three different radial locations. We can see that the fitted projections using the estimated detector response match the true projections very well.

IV. Future Works

The computer simulation has demonstrated that the proposed method can estimate detector response function in PET from point source measurements. We plan to apply the

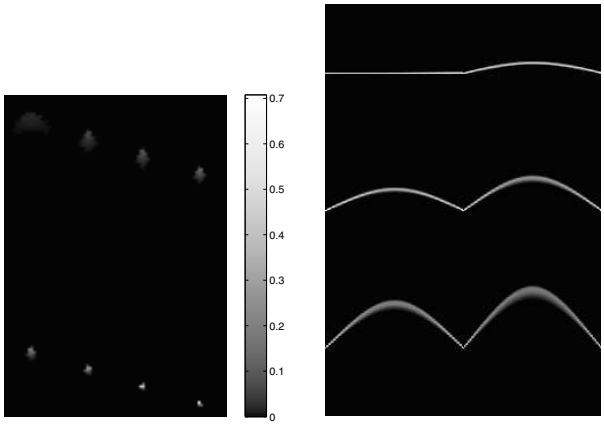

(a) (b)

Fig. 3. (a) Estimated detector response functions for eight selected radial bins. Top row: 7, 14, 21, 28; bottom row: 35, 42, 49, 56. Note bin 61 is at the radial center. (b) Fitted point source projections using the estimated detector response function at radial offsets of 0 mm, 10 mm, 20 mm, 30 mm, 40 mm, and 50 mm.

method to real data and to incorporate the estimated detector response functions into the Bayesian image reconstruction algorithm that we have developed [6]. In future work we will extend the method to PET systems with block detectors and to fully 3D PET reconstruction.

REFERENCES

[1] E. P. Ficaro, J. A. Fessler, P. D. Shreve, J. N. Kritzman, P. A. Rose, and J. R. Corbett, "Simultaneous transmission/emission myocardial perfusion tomography : Diagnostic accuracy of attenuation-corrected 99mTc-Sestamibi single-photon emission computed tomography," *Circulation*, vol. 93, no. 3, pp. 463–473, 1996.

[2] E. P. Ficaro and J. R. Corbett, "Advances in quantitative perfusion spect imaging," *J Nucl Cardiol*, vol. 11, pp. 62–70, 2004.

[3] V. Y. Panin, F. Kehren, H. Rothfuss, D. Hu, C. Michel, and M. E. Casey, "Pet reconstruction with system matrix derived from point source measurements," in *IEEE Nuclear Science Symposium Conference Record*, J. A. Seibert, Ed., 2004, pp. 2483–2487.

[4] L. R. Furenlid, D. W. Wilson, C. Yi-chun, K. Hyunki, P. J. Pietraski, M. J. Crawford, and H. H. Barrett, "Fastspect ii: a second-generation high-resolution dynamic spect imager," *IEEE Transactions on Nuclear Science*, vol. 51, no. 3, pp. 631–5, 2004.

[5] E. Mumcuoglu, R. Leahy, S. Cherry, and E. Hoffman, "Accurate geometric and physical response modeling for statistical image reconstruction in high resolution PET," in *Proc. IEEE NSS-MIC*, Anaheim, CA, 1996, pp. 1569–1573.

[6] J. Qi, R. M. Leahy, S. R. Cherry, A. Chatziioannou, and T. H. Farquhar, "High resolution 3D Bayesian image reconstruction using the microPET small animal scanner," *Phys Med Bio*, vol. 43, no. 4, pp. 1001–1013, 1998.

[7] A. R. Formiconi, A. Pupi, and A. Passeri, "Compensation of spatial system response in SPECT with conjugate gradient reconstruction technique," *Phys Med Bio*, vol. 34, no. 1, pp. 69–84, 1989.

[8] D. R. Gilland, R. J. Jaszczak, H. Wang, T. G. Turkington, K. L. Greer, and R. E. Coleman, "A 3D model of non-uniform attenuation and detector response for efficient iterative reconstruction in SPECT," *Phys Med Bio*, vol. 39, pp. 547–561, 1994.

[9] C. Tocharoenchai, B. M. W. Tsui, D. P. Lewis, E. C. Frey, and X. Zhao, "Compensation for the response function of medium energy collimator in ^{67}Ga planar and SPECT imaging," in *Proc. IEEE NSS-MIC*, 1998, pp. 1405–1408.

[10] A. M. Alessio, P. E. Kinahan, and T. K. Lewellen, "Modeling and incorporation of system response functions in 3D whole body PET," in *Proc. IEEE NSS-MIC*, 2004, pp. 3992–3996.

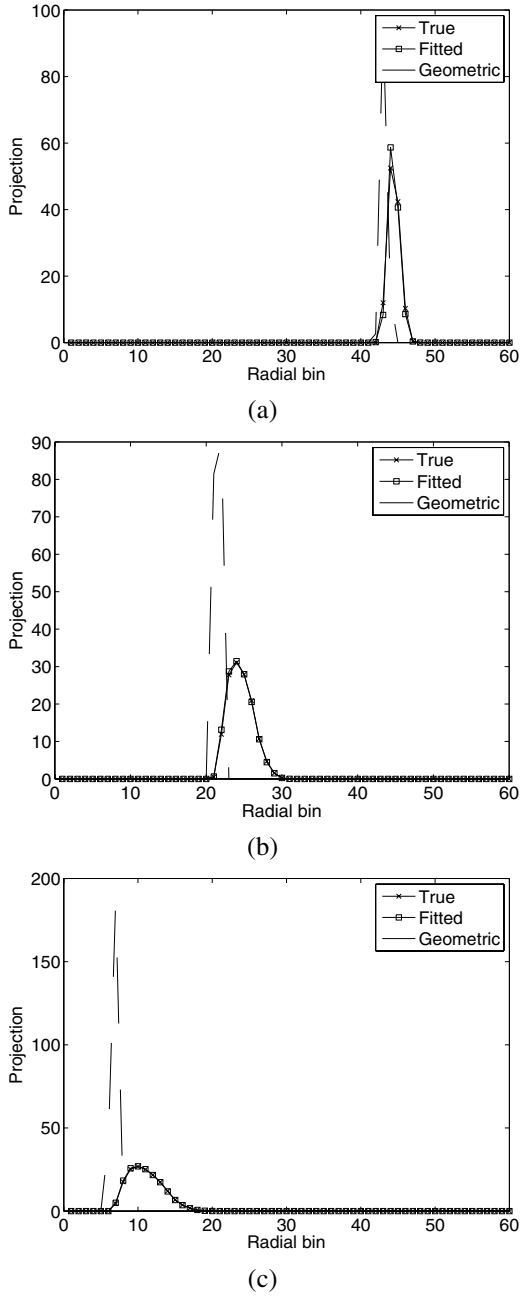

Fig. 4. Comparison of radial profiles of the true projection, geometric projection, and fitted projection of a point source at three different radial locations: (a) 10 mm; (b) 20 mm; and (c) 26 mm.

[11] A. Alessio, P. Kinahan, R. Harrison, and T. Lewellen, "Measured spatially variant system response for PET image reconstruction," in *Proc. IEEE NSS-MIC*, vol. 4, 2005, pp. 1986–1990.

[12] T. Frese, N. C. Rouze, C. A. Bouman, K. Sauer, and G. D. Hutchins, "Quantitative comparison of fbp, em, and bayesian reconstruction algorithms for the indypet scanner," *Ieee Transactions on Medical Imaging*, vol. 22, no. 2, pp. 258–276, 2003.

[13] F. J. Beekman, E. T. P. Slijpen, H. de Jong, and M. A. Viergever, "Estimation of the depth-dependent component of the point spread function of spect," *Med Phys*, vol. 26, no. 11, pp. 2311–22, 1999.

[14] R. H. Huesman, G. J. Klein, W. W. Moses, J. Qi, B. W. Reutter, and P. R. G. Virador, "List mode maximum likelihood reconstruction applied to positron emission mammography with irregular sampling," *IEEE Trans Med Im*, vol. 19, pp. 532–537, 2000.